Lithography-induced hydrophobic surfaces of silicon wafers with excellent anisotropic wetting properties

Jiajing Zhu[1], Yanling Tian[1,2], Xianping Liu[1], Chengjuan Yang[2]

1 School of Engineering, University of Warwick, Coventry, CV4 7AL, UK

2 Key Laboratory of Mechanism Theory and Equipment Design of Ministry of Education, Tianjin University, Tianjin 300072, China

Abstract:

In recent years, hydrophobic surfaces have attracted more and more attentions from many researchers. In this paper, we comprehensively discussed the effects of specific parameters of microstructures on the wetting properties by using the theoretical models, the effects of microstructures on two-dimensional anisotropic properties and the water droplet impact experiment. Firstly, the relationships between the CAs and variable parameters were explored after the formula derivation for three various patterns. Then three different patterns were fabricated successfully on the silicon wafers by lithography technology and the effects of microstructures (including LWD parameters and interval parameters) on surface wettability were studied based on the theoretical research. After that, the effects of microstructures on two-dimensional anisotropic properties were also studied. Finally, the water droplet impact experiment was carried out and the viscoelastic properties were simply investigated. Our research proposed a potential method for fabricating hydrophobic surfaces with excellent anisotropic properties. This method may be widely used in a variety of academic and industrial applications in the future.

Keywords: Lithography; Wettability; Hydrophobic; Anisotropic; Viscoelastic.

1 Introduction

Hydrophobic surfaces have attracted more and more attentions from many researchers because of the potential applications in academic and industrial fields. It has been reported that hydrophobic surfaces can be applied in water-repellence, diverse adhesion even tunable wettability, optical performance, magnetism, anti-bacterial, transparency, self-cleaning, antifogging, antireflection, low drag and great stability and durability, and so on.

In recent years, the research regarding to the hydrophobic surfaces mainly divided into two aspects: natural hydrophobic surfaces and artificial hydrophobic surfaces (which also written in biomimetic hydrophobic surfaces by some researchers). The artificial hydrophobic surfaces are always fabricated by diversity technologies in order to imitate the micro-/nano-structures from some plants and animals in nature.

During the early study period, researcher mainly focused on finding the natural hydrophobic surfaces and studying the morphology of their micro-/nano-structures. The “lotus effect” was firstly reported by Barthlott and Neinhuis [Barthlott et al. 1997], who revealed that lotus leafs have excellent superhydrophobic performance and self-cleaning features. Then the micro-/nano-structures of lotus leafs were studied by many researchers [Feng et al. 2002; Wang et al. 2014]. After that, other various natural hydrophobic surfaces with multifunction were discovered quickly. These natural hydrophobic surfaces mainly classified by the morphology of microstructures, which including array structures, sheet overlapped, high density hairs and seta shaped [Gao et al. 2017]. It mainly involved many plants and animals in nature, like the mosquito eyes [Gao et al. 2010], cicada wings [Zhang et al. 2006], butterfly wings [Zheng et al. 2007], rice leaf [Bixler et al. 2013], gecko foot [Liu et al. 2012], salvinia paradox [Barthlott et al. 2010], water strider [Feng et al. 2007], filefish skin [Cai et al. 2014] and so on.

With the rapid development of advanced technology, there is a popular trend to fabricate various micro-/nano-structures with different materials for artificial hydrophobic surfaces. A variety of materials were used to imitate the micro-/nano-structures from nature plants and animals. In general, it can be classified by metal materials (include Fe, Cu, Al, Ti, Zn, Mg, Ni et al.) and oxide metal

materials (include TiO2, ZnO, Al2O3, Fe3O4 et al.), polymer materials (include PDMS, PET, PEEK, PMMA et al.), silicon wafers and silica materials, carbon fibers, ceramics and so on. What's more, there are a large number of fabrication methods for hydrophobic surfaces have been researched in the past few years, including lithography technology [Zhang et al. 2009; Zhu et al. 2017; Vasilii et al. 2018], electrochemical technology [Kahng et al. 2001], chemical etching technology[He et al. 2011; Yang et al. 2014; Kim et al. 2009], chemical modification methods[Chen et al. 2010; Li et al. 2016; Zhang et al. 2011], mechanical processing technology [Arifvianto et al. 2011], laser ablation technology [Zhu et al. 2018; Doll et al. 2016; Yong et al. 2014; Bizi-bandoki et al. 2013], ultrasonic embossing technology [Zhu et al. 2017]and so on. These fabrication methods are mainly by means of changing the surface wetting properties, which can be divided into increasing the surface roughness with hierarchical micro-/nano-structures and lowing the surface energy by modifying chemical composition. Some researchers also attempted to combine two methods for the fabrication of higher hydrophobic surfaces and super-hydrophobic surfaces by increasing the surface roughness and lowing the surface energy simultaneously [He et al. 2011; Yang et al. 2014; Zhu et al. 2018; Zhu et al. 2017].

However, the effects of specific parameters of microstructures on the wetting properties, the effects of microstructures on two-dimensional anisotropic properties and the water droplets impact experiment were rarely studied meantime in previous research. In this paper, we comprehensively analyzed these contents. Firstly, four classic theoretical models were introduced and the formula derivation for three patterns were deduced. Then the relationships between the CAs and variable parameters were explored after the formula derivation. Based on the theoretical research, three different patterns were fabricated successfully on the silicon wafers by lithography technology and the effects of microstructures (including LWD parameters and interval parameters) on surface wettability were investigated. After that, the effects of microstructures on two-dimensional anisotropic properties were also studied. Finally, the water droplet impact experiment was carried out and simply discussed in this paper.

2 Materials and methods

2.1 Material details

The substrates used in this study were P-type silicon wafers (100) with size of 4 inch and thickness of 1mm. All the silicon wafers were polished and cleaned by removing contamination before the experiment. In this paper, silicon wafers were fabricated with three types of patterns, which included linear patterns, square patterns and dot patterns. We denoted that LWD parameters represent the dimension of convex area for three patterns, which include the lengths of square patterns, the widths of linear patterns and square patterns, the diameters of dot patterns. Then the interval parameters express the spacing dimension between the neighboring convex patterns. The specific characterization were explained in the Fig.1. From the Fig.1, variable *a* describe the widths of linear patterns and square patterns, the lengths of square parameters and the diameters of dot patterns. Variable *l* represent the lengths of linear patterns. Variable *b* reflect the interval values while variable *h* demonstrate the depths of these patterns. So the LWD parameters were denoted by *a* while the interval parameters were represented by *b*.

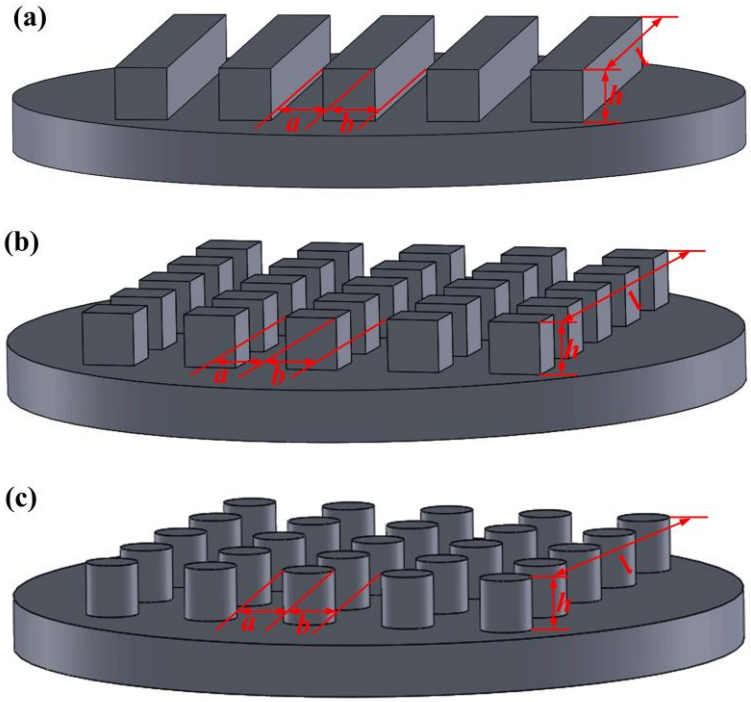

Fig.1. Schematic images for three patterns: (a) linear patterns; (b) square patterns; (c) dot patterns.

2.2 Fabrication methods

Lithography has become the initial technology for the surface modification because of its accurate and wonderful morphology for surfaces, which benefits for the research regarding to the effects of specific parameters of microstructures on the wetting properties. In this paper, the lithography technology was applied for the fabrication of various patterns with high quality and precision. The patterns were transferred from a photolithographic mask to a photoresist on the silicon wafer's surface successfully in the end. To be more specific, the silicon wafer was placed in the spin coater de-vice (EVG101CS from Australia) to gelatinize uniformly after drying process of 20 minutes in the drier machine. After the photoresist (EPG 535) on the silicon wafers was baked, it was put in the mask aligner (ABM 350 from America) to start exposure for 8s. Then it was placed in a beaker with the developer solution (5% NaOH solution) for 15s. After the etching process, the photoresist was fully removed and the designed patterns with the depth of nearly 80μm were fabricated perfectly on the silicon wafers.

2.3 Surface characterization

The surface morphology of patterned silicon surfaces with different LWD parameters and interval parameters were observed by Leica Microscope (Leica Microsystems from Germany: DM2700M) while 3D images were obtained by using a white light confocal microscope (Bruker from America). The images of surface viscoelasticity properties were captured by high speed camera. Besides, the VCA optima (AST PRODUCTS.INC from America) was used in this experiment to measure the CAs (values of contact angles) of patterned surfaces for the wettability evaluation. A distilled water-drop of 3 μL was used for the measurement of the contact angles. In order to ensure the reliability of data, at least three various locations were measured on the same patterns. Additionally, the water droplet impact experiment was also analyzed in this paper for the surface characterization.

3 Results and discussion

3.1 Theoretical analysis

In general, there are mainly four classic models to demonstrate the surface wetting properties (shown in the Fig.2). Young's model evaluates the wetting properties of the flat surfaces while Wenzel model, Cassie model and Wenzel-Cassie model reveal the wetting properties of the rough surfaces. From the previous literatures [Young et al. 1805; Wenzel et al. 1936; Cassie et al. 1994], the formulas of these classic models were listed as follow.

Young's Model:

$$\cos\theta = \frac{\gamma_{SA} - \gamma_{SL}}{\gamma_{LA}} \quad (1)$$

Wenzel Model:

$$\cos\theta_W = \frac{r(\gamma_{SA} - \gamma_{SL})}{\gamma_{LA}} = r\cos\theta \quad (2)$$

Cassie Model:

$$\cos\theta_C = f_1\cos\theta_1 + f_2\cos\theta_2 = f_1(1+\cos\theta_1) - 1 \quad (3)$$

Wenzel-Cassie Model:

$$\cos\theta_{W-C} = rf_1\cos\theta_1 - f_2 \quad (4)$$

Among these formulas, γ_{SA} is the solid-air interfacial energy; γ_{SL} is the solid-liquid interfacial energy; γ_{LA} is the liquid-air interfacial energy. Variable *r* represent the roughness factor, which was determined by the surface ratio of the actual surface are (S_1) and geometric surface area (S_2). f_1 demonstrate the total area of solid-liquid interface and f_2 express the total area of liquid-air interface in a plane geometrical area of unity parallel to the rough surface. Owing to the $f_1 + f_2 = 1$ and $\cos\theta_2 = -1$, the Cassie model can be simplified. θ represent the apparent contact angle in the flat surface. θ_W, θ_C and θ_{W-C} imply the contact angle in the rough surface under the Wenzel model, Cassie model and Wenzel-Cassie model respectively. θ_1 and θ_2 are the intrinsic contact angles for the solid-liquid interface and liquid-air interface.

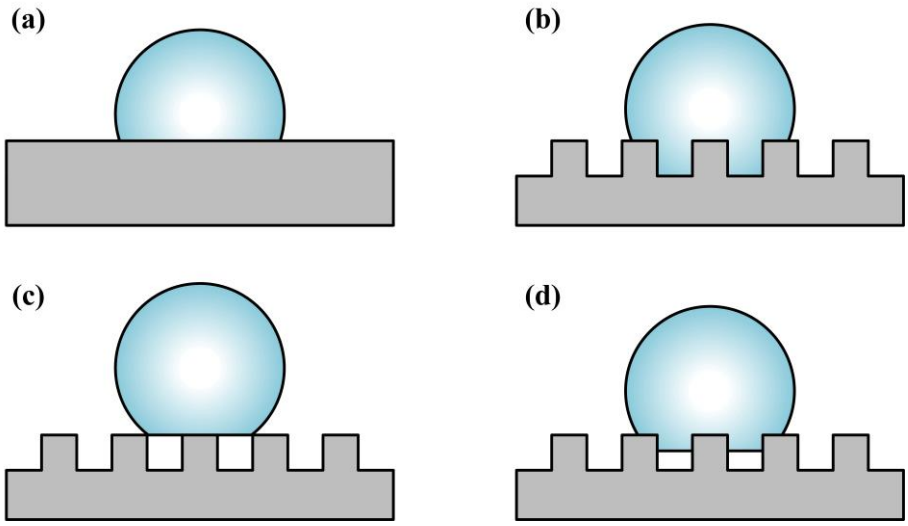

Fig.2. Four classic theoretical models: (a) Young's model; (b) Wenzel model; (c) Cassie model; (d) Wenzel-Cassie model.

Due to the various patterns on the samples, the rough surfaces were applied in our experiment. Based on the Wenzel model, Cassie model and Wenzel-Cassie model, we explicated the theoretical formula derivation for three patterns on the silicon wafers. From Fig.1, variable *a* describe the widths of linear patterns and square patterns, the lengths of square parameters and the diameters of dot patterns. Variable *l* represent the lengths of linear patterns. Variable *b* reflect the interval values while variable *h* demonstrate the depths of these patterns. Below are the specific derivation process.

Firstly, three models were used for discussing the wettability properties for the linear patterns.

Wenzel model:

$$\mathrm{r} = \frac{S_1}{S_2} = 1 + \frac{2h}{a+b} \quad (5)$$

$$\cos\theta_W = r\cos\theta = \left(1 + \frac{2h}{a+b}\right)\cos\theta \quad (6)$$

Cassie model:

$$f_1 = \frac{S_3}{S_4} = \frac{a}{a+b} \quad (7)$$

$$\cos\theta_c = f_1(\cos\theta + 1) - 1 = \frac{a}{a+b}(\cos\theta + 1) - 1 \quad (8)$$

Wenzel-Cassie model:

$$\cos\theta_{W-C} = \mathrm{r}f_1\cos\theta_1 + f_1 - 1 = \left(\frac{a}{a+b} + \frac{2ah}{(a+b)^2}\right)\cos\theta_1 + \frac{a}{a+b} - 1 \quad (9)$$

Secondly, we used the three models to evaluate the wettability properties for the square patterns.

Wenzel model:

$$\mathrm{r} = \frac{S_1}{S_2} = 1 + \frac{4ah}{(a+b)^2} \quad (10)$$

$$\cos\theta_W = r\cos\theta = \left(1 + \frac{4ah}{(a+b)^2}\right)\cos\theta \quad (11)$$

Cassie model:

$$f_1 = \frac{S_3}{S_4} = \frac{a^2}{(a+b)^2} \quad (12)$$

$$\cos\theta_c = f_1(\cos\theta + 1) - 1 = \frac{a^2}{(a+b)^2}(\cos\theta + 1) - 1 \quad (13)$$

Wenzel-Cassie model:

$$\cos\theta_{W-C} = \mathrm{r}f_1\cos\theta_1 + f_1 - 1 = \left(1 + \frac{4ah}{(a+b)^2}\right)\frac{a^2}{(a+b)^2}\cos\theta_1 + \frac{a^2}{(a+b)^2} - 1 \quad (14)$$

Thirdly, we introduced the three models when used for assessing the wettability properties for the dot patterns.

Wenzel model:

$$\mathrm{r} = \frac{S_1}{S_2} = 1 + \frac{\pi ah}{(a+b)^2} \quad (15)$$

$$\cos\theta_W = r\cos\theta = \left(1 + \frac{\pi ah}{(a+b)^2}\right)\cos\theta \quad (16)$$

Cassie model:

$$f_1 = \frac{S_3}{S_4} = 1 - \frac{\pi a^2}{4(a+b)^2} \quad (17)$$

$$\cos\theta_c = f_1(\cos\theta + 1) - 1 = \left(1 - \frac{\pi a^2}{4(a+b)^2}\right)(\cos\theta + 1) - 1 \quad (18)$$

Wenzel-Cassie model:

$$\cos\theta_{W-C} = \mathrm{r}f_1\cos\theta_1 + f_1 - 1 = \left(1 + \frac{\pi ah}{(a+b)^2}\right)\left(1 - \frac{\pi a^2}{4(a+b)^2}\right)\cos\theta_1 + \frac{\pi a^2}{4(a+b)^2} \quad (19)$$

From the formula derivation, some conclusions can be summarized. When the concave area were filled with the bottom of the water droplets and in the state of the Wenzel model, the values of the contact angles (θ) are closely related to the variables of a, b and h. In the state of the Cassie model, the values of the contact angles (θ) are relevant to the variables of a, b but not relevant to the variable of h. In the

Wenzel-Cassie model state, the values of the contact angles (θ) are also affected by the variables of a, b and h. Based on these deductions, the surface wetting properties can be partly explained to some extent.

3.2 Surface morphology analysis

In order to investigate the effects of various microstructures on surface wettability, experiments were carried out with three types of patterns, which including linear patterns, square patterns and dot patterns. The three different patterns were designed with uniformed distribution and ununiformed distribution respectively. But the depths of patterns (h) were set as same in our experiment. The former one means that the proportion of the convex area and concave area was 1:1. So the LWD parameters was set to be equal to the interval between the two patterns in the former experiment. Additionally, LWD parameters were designed to be 500μm, 200μm, 100μm and 50μm respectively. The surface morphology of patterned silicon surfaces with multiple parameters were observed by Leica Microscope (Leica Microsystems from Germany: DM2700M) and 3D profiles were examined by a white light confocal microscope (shown in Fig.3).

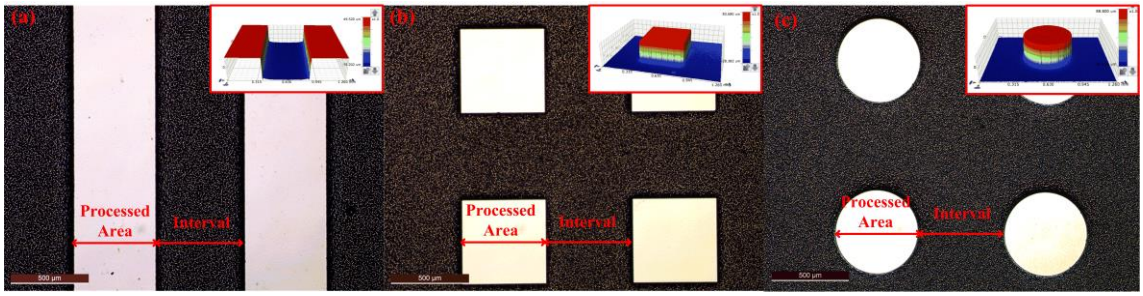

Fig.3. 2D images and 3D images of surface morphology: (a) linear patterns with LWD=500μm; (b) square patterns with LWD=500μm; (c) dot patterns with LWD=500μm.

Besides, the interval between neighboring linear patterns, square patterns and dot patterns also influenced the surface morphology. In the latter experiment, the proportion of the convex area and concave area were 2:1, 1:1, 2:3, 1:2 and 2:5. LWD parameters were 60 μm while the interval of two neighboring lines, squares and dots were set to be 30μm，60μm，90μm，120μm and 150μm respectively.

From the Fig.3, it indicated that we can obtain perfect microstructures successfully on silicon wafers by lithography technology. There were no obvious

defects and damages on microstructures from the 2D images of surface morphology. Additionally, the sidewalls of microstructures were straight and there were no tilted slopes from the 3D images of surface morphology. Because of the etching process as we noted before, the sidewalls of microstructures and the bottom surfaces of the concave area were lightly rough while the top surfaces of the convex area were plat and smooth.

3.3 Effect of microstructures on surface wettability

3.3.1 Effect of LWD parameters on surface wettability

In this experiment, the proportion of the convex area and the concave area was 1:1. LWD parameters were designed to be 500μm, 200μm, 100μm and 50μm respectively, which were equal to the interval values. The contact angles were measured by VCA optima (AST PRODUCTS.INC from America) and the duration of measurement was ten days. After this period, the surfaces wettability became stability and there were almost no changes for the contact angles.

The evolution of contact angles over time for LWD parameters regarding to the linear patterns, square patterns and dot patterns were shown in Fig.4 (a), (b) and (c). It can be seen that the contact angles of all the patterned surfaces fluctuated in a certain range. From the Fig.4 (a), (b) and (c), we can see that the variation ranges of contact angles for linear patterns, square patterns and dot patterns were 78°~122°, 66.5°~146°and 70.8°~145.6° respectively. It can be concluded that the overall CAs of linear patterns were smallest by compared with CAs of square patterns and dot patterns. The different types of three various patterns may be the main reason to cause this phenomenon. Within the same area, the distribution of square patterns and dot patterns were more intensive and had higher surface roughness than linear patterns. Therefore, the square patterned and dot patterned surfaces preferred to have higher hydrophobicity than the linear patterned surfaces.

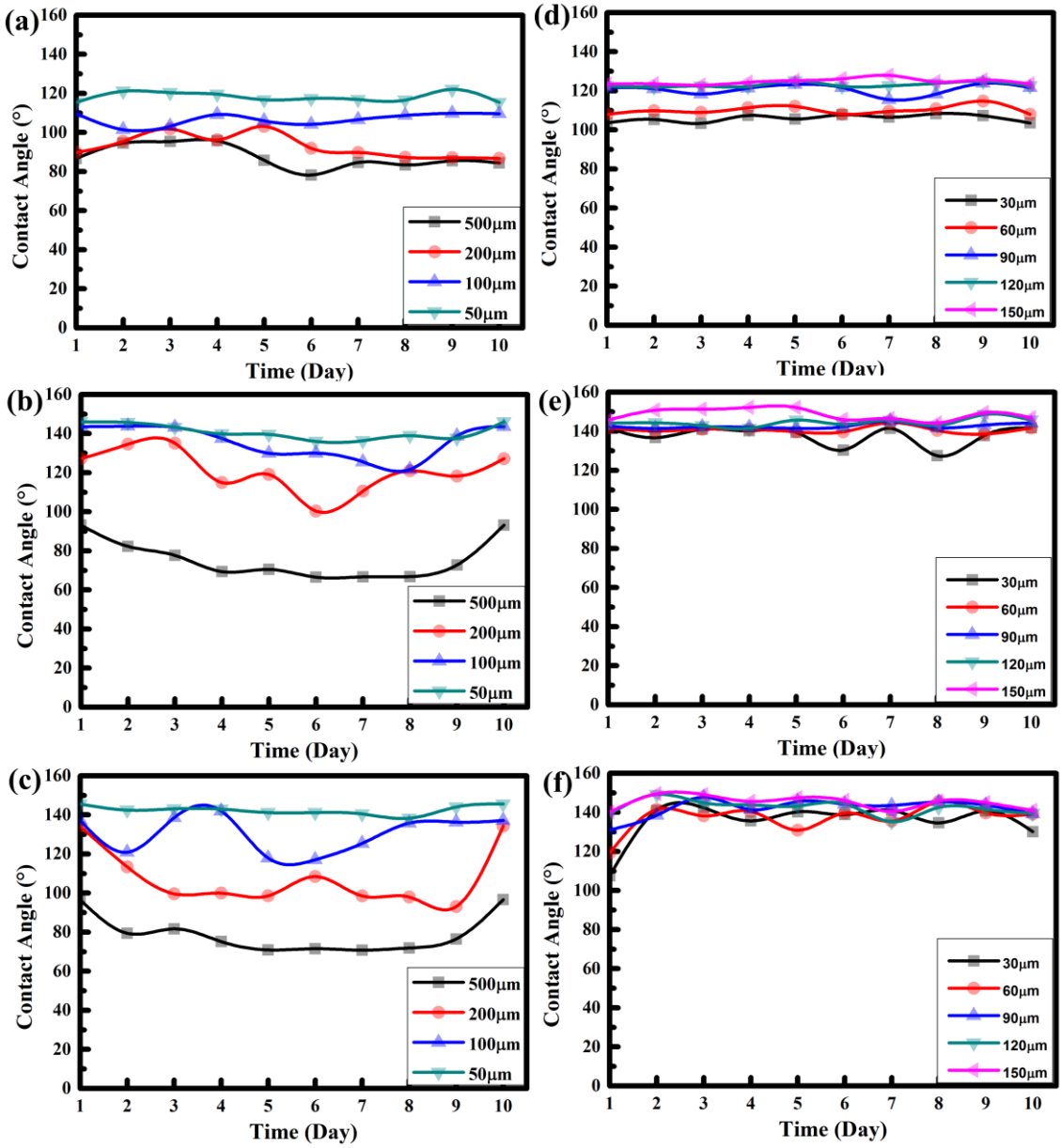

Fig.4. Evolution of contact angles over time for (a) linear patterns (LWD parameters); (b) square patterns(LWD parameters); (c) dot patterns(LWD parameters); (d) linear patterns(Interval parameters); (e) square patterns(Interval parameters); (f) dot patterns(Interval parameters).

Besides, the CAs of various patterns increased as the LWD parameters decreased. To be more specific, when the LWD parameters were below 100μm, the contact angles were lager than 90° and the wettability of surfaces changed from hydrophilic to hydrophobic simultaneously. What's more, the best wettability surfaces were obtained when the LWD parameters were equal to 50μm.

From the Fig.5 (a), we can see that the CA (value of the contact angle) of silicon wafers without microstructures was 87.3°. Then the images of contact angles of

silicon wafers with LWD=50μm were shown in Fig.5 (b), (c) and (d) and corresponding CAs were 122.05°, 146°, 145.6° for linear patterns, square patterns and dot patterns respectively. So the hydrophilic surfaces for silicon wafers transformed to the higher hydrophobic surfaces successfully by using lithography technology.

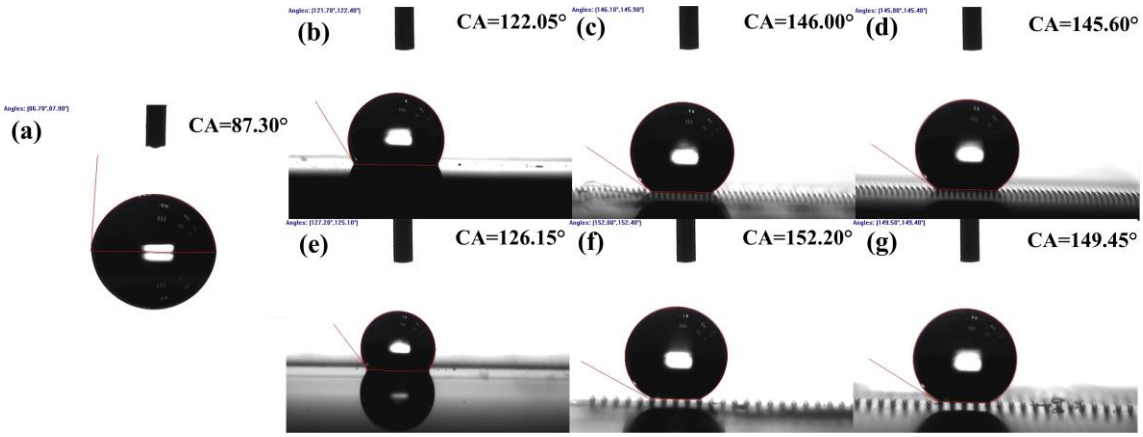

Fig.5. Images of contact angles of silicon wafers. (a) Contact angle of silicon without microstructures; (b) Contact angle of linear patterns (LWD=50μm); (c) Contact angle of square patterns (LWD=50μm); (d) Contact angle of dot patterns (LWD=50μm) (e) Contact angle of linear patterns (Interval=150μm); (f) Contact angle of square patterns (Interval=150μm); (g) Contact angle of dot patterns (Interval=150μm).

3.3.2 Effect of interval parameters on surface wettability

In the latter experiment, the proportion of the convex area and concave area were 2:1, 1:1, 2:3, 1:2 and 2:5. LWD parameters were 60 μm while the interval of two neighboring lines, squares and dots were set to be 30μm，60μm，90μm，120μm and 150μm respectively. The contact angles were measured by VCA optima (AST PRODUCTS.INC from America) and the duration of measurement was ten days. After this period, the surfaces wettability became stability and there were almost no changes for the contact angles.

The evolution of contact angles over time for interval parameters regarding to the linear patterns, square patterns and dot patterns were shown in Fig.4 (d), (e) and (f). It can be seen that the contact angles of all the patterned surfaces fluctuated in a certain range. From the Fig.4 (d), (e) and (f), we can see that the variation ranges of contact

angles for linear patterns, square patterns and dot patterns were 103.5 °~ 127.85 °, 127.45 ° ~152.15 ° and 107.5 ° ~ 149.45 ° respectively. It can be concluded that the overall CAs of linear patterns were still less than the CAs of square patterns and dot patterns, which was consistent with the obtained results of Section 3.2.1.

It can be seen from the Fig.4 that the values of all CAs were larger than 90°, which means that hydrophobic surfaces can be fabricated successfully in this method. The explanation for this phenomenon may due to the LWD parameters were all designed to be 60μm. According to above experiment results of Section 3.2.1, when the basic size of a pattern was smaller than 100μm, the hydrophobic surfaces were more easily to be obtained.

In addition, as the interval parameters rose, the corresponding contact angles increased as well. The reasons for this phenomenon may be due to the volume of water droplets and depths of microstructures. In our experiment, the volume of a water droplet was 3μl with a diameter of about 894.7μm, which was much larger than the LWD parameters (60μm) and interval parameters (varied from 30μm to 150μm). So a water droplet was dripped on several convex areas and some concave areas. What's more, the depths of microstructures were deeper than regular research and the value was over 80μm. According to the Wenzel-Cassie model, the depths of microstructure were also another important parameter to influence the surface wettability properties. When the depths and interval were larger, there were more air in the cavities to support the water droplet. So the water droplet was less likely to fall into the cavities and we preferred to obtain the hydrophobic surfaces with higher CAs.

From the Fig.5 (a), (e), (f) and (g), we can see that the CAs of silicon wafers increased from 87.3° for polished surfaces to 126.15°, 152.2°, 149.45° for linear patterns, square patterns and dot patterns respectively when the interval parameter was equal to 150μm. Finally, we obtained the hydrophobic surfaces successfully from the hydrophilic surfaces and some surfaces even changed to the super-hydrophobic surfaces.

3.3.3 Discussions regarding to the surface wetting properties

As we investigated in the Section 3.1, it indicated the relationships between the

different parameters and three theoretical models. In the states of the Wenzel model and Wenzel-Cassie model, the values of the contact angles (θ) are closely related to the variables of *a*, *b* and *h*. However, in the state of the Cassie model, the values of the contact angles (θ) are relevant to the variables of *a*, *b* but not relevant to the variable of *h*. What's more, LWD parameters denote *a* while interval parameters means *b*. The values of *h* were set as same in our experiment. So the LWD parameters and the interval parameters were both important for the surface wettability no matter what kind of models.

On the one hand, the effect of various shape of three patterns on the surface wettability was discussed. From Fig.5 (b) and (e), we can see that the linear patterns were both in the state of the Wenzel model and the concave area were filled with the bottom of the water droplets. However, the square patterns and dot patterns were in the state of Wenzel-Cassie model when LWD=50 μm, shown in Fig.5 (c) and (d). What's more, the square patterns and dot patterns were in the state of Cassie model when interval=150 μm, shown in Fig.5 (f) and (g). So it can be concluded that the linear patterns were harder than the square patterns and dot patterns to obtain the higher CAs. The Cassie model is more likely to have the higher CAs while the Wenzel model is rarer to have the higher CAs.

On the other hand, the effect of various LWD parameters and interval parameters on the surface wettability was analyzed. From the Fig.4, it can be seen that the CAs increased as the LWD parameters decreased. It can be corresponding to all the three theoretical models in the Section 3.1. When variable *a* (LWD parameters) decreased, the values of θ preferred to have the larger values. But when the interval parameters *b* increased, the CAs also increased in our experiment. This phenomenon was a little different from the theoretical deduction. So we considered the effect of the depths of patterns (*h*) on this phenomenon. As we known, the CAs were related to the depths of patterns (*h*) under the Wenzel-Cassie model and Wenzel model while CAs were not related to the depths of patterns (*h*) under the Cassie model. We proposed that the CAs may be influenced by the volume of water droplet and volume of the concave area. We suggested that when the values of depth and interval parameters were larger,

there were more air in the cavities to support the water droplet. In that case, the water droplet was less likely to fall into the cavities and prefer to be in the state of the Cassie model or the Wenzel-Cassie model. Therefore, it is more likely to obtain the hydrophobic surfaces with higher CAs when the interval parameters increased in our practical experiment.

3.4 Effect of microstructures on two-dimensional anisotropic properties

Additionally, the relationships between the microstructures and two-dimensional anisotropic properties were also researched in our studies. The LWD parameters and interval parameters were analyzed separately. The values of CAs differences were calculated by the absolute differences between the parallel CAs and vertical CAs. The parallel direction was defined as along to the groove for linear patterns, perpendicular to the interval increase side for square patterns and dot patterns. The vertical direction is obtained by rotating 90° from the parallel direction of these fabricated surfaces.

From the Fig.6 (a), we can see that the values of the contact angles had an increase trend with the decrease of the LWD parameters. The proportion of the concave area and convex area was 1:1 as LWD parameters was set to be equal to the interval between the two patterns. In this experiment, LWD parameters were designed to be 500μm, 200μm and 100μm, as shown in Fig.6 (a) with l1/s1/d1, l2/s2/d2, l3/s3/d3 and l4/s4/d4 respectively.

As shown in Fig.6 (b), we can see that the values of the contact angles rose first and then dropped with the increase of the interval parameters. The proportion of the concave area and convex area were 2:1, 1:1, 2:3, 1:2 and 2:5. LWD parameters were 60 μm while the interval of two neighboring lines, squares and dots were set to be 30μm ,60μm ,90μm ,120μm and 150μm, as show in Fig.6 (b) with l5/s5/d5, l6/s6/d6, l7/s7/d7, l8/s8/d8 and l9/s9/d9 respectively.

By comparing the Fig.6 (a) and (b), the effects of LWD parameters and interval parameters with same shape of patterns on the two dimensional anisotropic properties were limited. The interval parameters have more significant influence on the absolute CAs differences for linear patterns. Because the values of CAs differences regarding

to the LWD parameters (11.9°~16.55°) were smaller than that of the interval parameters (18.85°~20.95°).

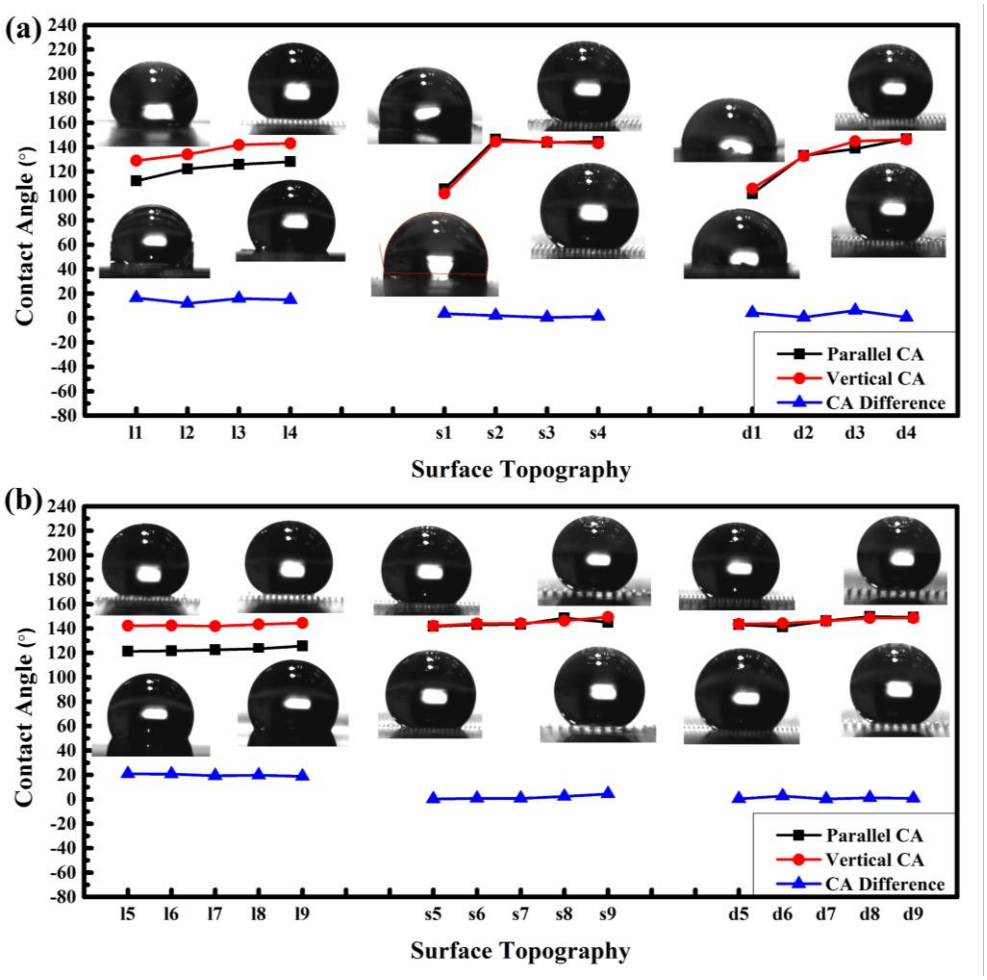

Fig.6. Variation trend of CAs on two-dimensional anisotropic wetting. (a) The effect of LWD parameters on anisotropic properties; (b) The effect of interval parameters on anisotropic properties.

What's more, the absolute CAs differences on two dimensional had shown little changes among the three patterns. From the Fig.6 (a) and (b), we can see that the parallel CAs were always smaller than the vertical CAs, especially for the linear patterns. For linear patterns, all the parallel CAs were smaller than the vertical CAs. However, it shown the uncertain regularity for square patterns and dot patterns. In that case, the linear patterns had the largest absolute CAs differences on the two dimensional anisotropic properties. The absolute CAs differences of linear patterns were the largest and the values were 11.9°~20.95°. The variation of absolute CAs differences of square patterns were below 5° while the variation of absolute CAs

differences of dot patterns were below 6.5°. So we can concluded that the various shapes of microstructures play an important role in the two dimensional anisotropic properties.

3.5 Analysis of the water droplet impact experiment

Recently, water droplet impact experiments (which also called the pancake bouncing dynamics by some researchers) are widely used to measure the surface viscoelastic properties. It is clear that the surface viscoelastic properties have a wide range of applications, which include anti-icing field, dropwise condensation field and self-cleaning field.

Water droplet impact experiments were conducted using a high-speed camera at the rate of 2000 frames per second. Snapshots in Fig.5 showed the viscoelastic behaviors of 7.5 μL water droplet on the squared surfaces. The water droplet was released automatically and immediately from a height of 6.0 cm above the surfaces after pressing the button. Then the water droplet began to touch the patterned surfaces after pressing the button. But in this experiment, we only pay more attention to the surface viscoelastic properties. In that case, we assumed that it would be t=0 ms in this paper when the water droplet began to touch the squared surfaces, which means the beginning of the water bouncing dynamics process.

Fig.7 showed the time evolution of a water droplet impact dynamics on the patterned surfaces (LWD=50 μm and interval=50 μm). On touching the surfaces at t=0 ms, the water droplets still remained the round shape during the dropping process. After that, the bottom of water droplet started to penetrate into the microstructures in a localized region. At t=4 ms, the water droplet reached a maximum lateral extension, which liked the pancake shape. Then the top of water droplet began to retract on the surfaces from 6 ms but didn't detach from the surfaces finally. Afterwards, the extended process and retractive process appeared repeatedly several times until the water droplet stopped moving and finally achieved to the steady state.

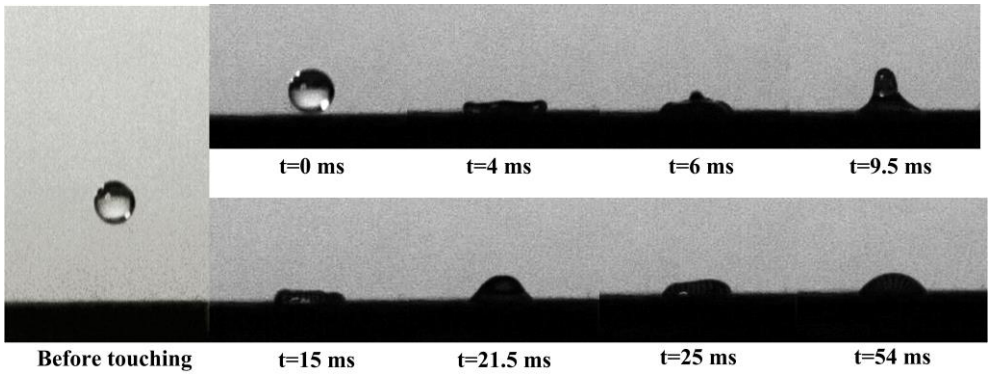

Fig.7 Time evolution of a water droplet impact dynamics on the squared surfaces (LWD=50 μm and Interval=50 μm).

From the results of the water droplet impact dynamics, we demonstrated that the extended process and retractive process were closely related to the capillary energy stored in the liquid. It might be affected by a wide range of factors, such as the volume of the water droplet, the height above the surfaces, impact velocity, air resistance, contact surfaces materials, the intermolecular force between the liquid and solid surfaces. So there are many complicated reasons to cause this phenomenon that we could see in Fig.7. From previous studies of other researchers, it showed that this surface viscoelastic properties in this experiment didn't perfect as we expected. The main reason can be quantified by the fabricated surface wetting abilities. However, in this paper, the purpose of the water droplet impact dynamics was just for the hydrophobic surface characterization. Therefore, we may explored more about the theories and applications for this field in the future works.

4 Conclusions

In this paper, three types of microstructure were fabricated with better quality and high precision, which included linear patterns, square patterns and dot patterns. Through the analysis of above results, some conclusions are summarized as follow:

(1) Lithography technology is an initial method for fabricating accurate microstructures and it has many advantages by compared with other processing methods. So it was a wise choice to obtain hydrophobic surfaces with better quality. From the 2D and 3D images of surface morphology, there were no obvious defects on microstructures and the sidewalls of microstructures were straight.

(2) Four classic theoretical models were introduced and the formula derivation for three patterns were deduced in our paper. Then the relationships between the CAs (θ) and variable parameters were explored after the formula derivation process. In the states of the Wenzel model and Wenzel-Cassie model, the values of the contact angles (θ) are closely related to the variables of *a*, *b* and *h*. However, in the state of the Cassie model, the values of the contact angles (θ) are relevant to the variables of *a*, *b* but not relevant to the variable of *h*.

(3) The effect of microstructures on surface wettability were measured and analyzed in our paper. Even though there were three types of patterned microstructure on silicon wafers in this research, the surface wettability still presented a similar regularity and its trend was basically similar. However, due to the different structural features, the overall average of linear patterns' contact angles were less than the those of square patterns' contact angles and dot patterns' contact angles.

(4) LWD parameters and interval parameters both have certain influence to the surface wettability of silicon wafers. The smaller LWD parameters obviously had higher CAs and preferred to show better hydrophobic surface, especially when the size is less than 100μm. When the dimension of microstructure was 60 μm, no matter how the interval parameters changed, the contact angle were all larger than 90°. In this case, all the patterned silicon surface had become a hydrophobic surface, and some of them even reached the super-hydrophobic state (larger than 150°).

(5) Effect of microstructures on two-dimensional anisotropic properties were also investigated in this paper. We mainly studied the effects of LWD parameters, interval parameters and various shapes of microstructures on the two dimensional anisotropic properties. The interval parameters have more significant influence on the absolute CAs differences for linear patterns. What's more, the linear patterns had the largest absolute CAs differences on the two dimensional anisotropic properties.

(6) The water droplets impact experiment was carried out and analyzed in this paper. From the results, the water droplet changed from the round shape to the pancake shape and finally achieved the steady semicircular shape during the dropped process. The top of water droplet tried to retract on the surfaces but didn't detach from

the surfaces finally. So it shows limited viscoelastic properties for fabricated silicon surfaces.

In summary, we proposed a potential method to fabricate hydrophobic surfaces with excellent anisotropic properties. This method may be widely used in various academic and industrial applications in the future.

Acknowledgments

This work was supported by China-EU H2020 International Science and Technology Cooperation Project (FabSurfWAR Nos.2016YFE0112100 and 644971) and National Natural Science Foundations of China [Nos.51405333, 51675371, 51675376 and 51675367]. The authors are particularly grateful to Tianjin University and Xian Jiaotong University for the technical support. Jiajing Zhu wish to gratefully acknowledge the financial support by China Scholarship Council.

References

Barthlott W, Neinhuis C (1997) Purity of the sacred lotus, or escape from contamination in biological surfaces. Planta 202:1–8.

Feng L, Li S, Li Y et al (2002) Super-hydrophobic surfaces: From natural to artificial. ADV MATER 14:1857–1860.

Wang G, Guo Z, Liu W (2014) Interfacial effects of superhydrophobic plant surfaces: A review. J BIONIC ENG 11:325–345.

Gao XY, Guo ZG (2017) Biomimetic Superhydrophobic Surfaces with Transition Metals and Their Oxides: A Review. J BIONIC ENG 14:401–439.

Gao X, Yan X, Yao X et al (2010) The dry-style antifogging properties of mosquito compound eyes and artificial analogues prepared by soft lithography. ADV MATER 19:2213–2217.

Zhang G, Zhang J, Xie G et al (2006) Cicada wings: A stamp from nature for nanoimprint lithography. SMALL 2:1440–1443.

Zheng Y, Gao X, Jiang L et al (2007) Directional adhesion of superhydrophobic butterfly wings. SOFT MATTER 3:178–182.

Bixler GD, Bhushan BF (2013). Fluid drag reduction and efficient self-cleaning with rice leaf and butterfly wing bioinspired surfaces. NANOSCALE 5:7685–7710.

Liu K, Du J, Wu J et al (2012) Superhydrophobic gecko feet with high adhesive

forces towards water and their bio-inspired materials. NANOSCALE 4:768–772.

Barthlott W, Schimmel T, Wiersch S et al (2010) The salvinia paradox: Superhydrophobic surfaces with hydrophilic pins for air retention under water. ADV MATER 22:2325–2328.

Feng X Q, Gao X, Wu et al (2007) Superior water repellency of water strider legs with hierarchical structures: Experiments and analysis. LANGMUIR 23:4892–4896.

Cai Y, Lin L, Xue Z et al (2014) Filefish inspired surface design for anisotropic underwater oleophobicity. ADV FUNCT MATER 24:809–816.

Zhang X, Zhang J, Ren Z et al (2009) Morphology and Wettability Control of Silicon Cone Arrays Using Colloidal Lithography. LANGMUIR 25:7375–7382.

Zhu JJ, Tian YL, Yang CJ et al (2017) Lithography-induced wettability Changes of Silicon. Shanghai: 2017 IEEE International Conference of Manipulation, Manufacturing and Measurement on the Nanoscale (3M-NANO).

Vasilii B, Valentina M, Artem K et al (2018) Hydrophilic/hydrophobic surface modification impact on colloid lithography: Schottky-like defects, dislocation, and ideal distribution. APPL SURF SCI 6:443–448.

Kahng B, Jeong H, Barabasi AL (2001) Quantum dot and hole formation in sputter erosion. APPL PHYS LETT 78:805–807.

He Y, Jiang CY, Yin HX (2011) Tailoring the wettability of patterned silicon sur-faces with dual-scale pillars: From hydrophilicity to superhydrophobicity. APPL SURF SCI 257:7689–7692.

Yang XM, Zhong ZW, Diallo EM et al (2014) Silicon wafer wettability and aging behaviors: Impact on gold thin-film morphology. MAT SCI SEMICON PROC 26:25–32.

Kim T, Tahk D, Lee HH (2009) Wettability-Controllable Super Water- and Moderately Oil-Repellent Surface Fabricated by Wet Chemical Etching. LANGMUIR 25:6576–6579.

Chen F, Zhang D, Yang Q (2010) Anisotropic wetting on microstrips surface fabricated by femtosecond laser. LANGMUIR 27:359–365.

Li H, Yu S, Han X (2016) A stable hierarchical superhydrophobic coating on pipeline steel surface with self-cleaning, anticorrosion, and anti-scaling properties. Colloid Surf. A-Physicochem. Eng. Asp. 503:43–52.

Zhang D, Chen F, Yang Q et al (2011) Mutual wetting transition between isotropic

and anisotropic on directional structures fabricated by femotosecond laser. SOFT MATTER 7:8337–8342.

Arifvianto B, Mahardika M, Dewo P (2011) Effect of surface mechanical attrition treatment (SMAT) on microhardness, surface roughness and wettability of AISI 316L. MATER CHEM PHYS 125:418–426.

Zhu JJ, Tian YL, Liu XP (2018) Rapid fabrication of super-hydrophobic surfaces of silicon wafers with excellent anisotropic wetting. MICROSYST TECHNOL 24:1–7.

Doll K, Fadeeva E, Stumpp N S (2016) Reduced bacterial adhesion on titanium surfaces micro-structured by ultra-short pulsed laser ablation. BioNanoMaterials 17:1–2.

Yong J, Yang Q, Chen F et al (2014) A simple way to achieve superhydrophobicity, controllable water adhesion, anisotropic sliding, and anisotropic wetting based on femtosecond-laser-induced line-patterned surfaces. J MATER CHEM A 2:5499–5507.

Bizi-bandoki P, Valette S, Audouard E (2013) Time dependency of the hydrophilicity and hydrophobicity of metallic alloys subjected to femtosecond laser irradiations. APPL SURF SCI 273:399–407.

Zhu JJ, Tian YL, Yang CJ, Liu XP (2017) Low-cost and fast fabrication of the ultrasonic embossing on polyethylene terephthalate (PET) films using laser processed molds. MICROSYST TECHNOL 23:5653–5668.

Young T (1805) An essay on the cohesion of fluids. PHILOS T ROY SOC A 95: 65–87.

Wenzel RN (1936) Resistance of solid surfaces to wetting by water. J IND ENG CHEM 28:988–994.

Cassie A, Baxter S (1994) Wettability of porous surfaces. Transactions of the Faraday Society 40:546–551.